



Geophysical Research Letters

RESEARCH LETTER

10.1029/2020GL088255

Key Points:

- Alkenone and TEX_{86} temperatures represent summer SST during the last glacial with low sea level (<-90 m)
- Isoprenoidal GDGT community structure index indicates a stratified upper ocean during glacial time
- Increasing tetraether lipid-based temperature indicates strengthening of the Tsushima Warm Current in the central Japan Sea in the Holocene

Supporting Information:

- Supporting Information S1

Correspondence to:

X. Shi,
xfshi@fio.org.cn

Citation:

Wu, Y., Shi, X., Gong, X., Jian, Z., Zou, J., Liu, Y., et al. (2020). Evolution of the upper ocean stratification in the Japan Sea since the last glacial. *Geophysical Research Letters*, 47, e2020GL088255. <https://doi.org/10.1029/2020GL088255>

Received 5 APR 2020

Accepted 29 JUL 2020

Accepted article online 4 AUG 2020

Evolution of the Upper Ocean Stratification in the Japan Sea Since the Last Glacial

Yonghua Wu^{1,2} Xuefa Shi^{1,2} Xun Gong³ Zhimin Jian⁴ Jianjun Zou^{1,2} Yanguang Liu^{1,2} Gerrit Lohmann³ Sergey A. Gorbarenko⁵ Ralf Tiedemann³, and Lester Lembke-Jene³

¹Key Laboratory of Marine Geology and Metallogeny, First Institute of Oceanography, Ministry of Natural Resources, Qingdao, China, ²Laboratory for Marine Geology, Pilot National Laboratory for Marine Science and Technology, Qingdao, China, ³Alfred-Wegener-Institut Helmholtz-Zentrum für Polar- und Meeresforschung, Bremerhaven, Germany, ⁴State Key Laboratory of Marine Geology, Tongji University, Shanghai, China, ⁵V.I. Il'ichev Pacific Oceanological Institute, Far East Branch of Russian Academy of Science, Vladivostok, Russia

Abstract Paleoceanographic evidence commonly indicates that Last Glacial Maximum surface temperatures in the Japan Sea were comparable to modern conditions, in striking difference to colder neighboring regions. Here, based on a core from the central Japan Sea, our results show similar $\text{U}^{37}\text{K}'$ - and TEX_{86} -derived temperatures between 24.7 and 16.3 ka BP, followed by an abrupt divergence at \sim 16.3 ka BP and a weakening of divergence after \sim 8.7 ka BP. We attribute this process to a highly stratified glacial upper ocean controlled by the East Asian Summer Monsoon, increasing thermal gradient between surface and subsurface layers during the deglaciation and the intrusion of Tsushima Warm Current since the mid-Holocene, respectively. Therefore, we suggest that threshold-like changes in upper-ocean temperatures linked to sea level rise and monsoon dynamics, rather than just sea surface temperatures, play a critical role in shaping the thermal and ventilation history of this NW Pacific marginal sea.

Plain Language Summary Abnormally warm surface ocean conditions in the Japan Sea during last glacial are a mystery in Pacific paleoenvironmental history. We analyzed records of $\text{U}^{37}\text{K}'$ - and TEX_{86} -derived temperatures from the central Japan Sea, which suggests an oceanographic evolution from a highly stratified glacial upper ocean, to a deglacial surface-subsurface thermal gradient control, and subsequently to modern well-ventilated conditions since the intrusion of the Tsushima Warm Current started after the mid-Holocene. Our results suggest a combination of critical factors of oceanographic change, rather than a stand-alone thermal feature, in changing the history in the Japan Sea.

1. Introduction

The Japan Sea (JS), as a semienclosed marginal sea of the northwest Pacific, is surrounded by the Eurasian Continent and the Japanese Islands (Figure 1). It is at present connected with the adjacent seas only by four shallow straits with sill depths of less than 135 m, and it is also located near multiple, both high- and low-latitude, climate and oceanographic action centers, such as the East Asian Summer and Winter Monsoon, and the North Pacific Western Boundary currents. As a result of its unique location and topography, it displays an extremely high sensitivity to changing environmental background conditions on geological to instrumental timescale, such as sea level and insolation change (Gorbarenko et al., 1995; Oba et al., 1991; Tada et al., 1999), variations in monsoonal thermal and precipitation properties (Fujine et al., 2009; Liu et al., 2014), and sea ice occurrence and deep water formation (Ikehara, 2003; Ikehara & Itaki, 2007), including future climate change (Gamo, 1999). Thus, the oceanographic conditions of the JS have not been static during the geological past but varied significantly. Changes in local, regional, or global climatic conditions caused a shift from a glacial, oceanographically largely sealed-off marginal sea to the modern well ventilated, relatively nutrient-poor basin (e.g., Lohmann et al., 2019).

During the Last Glacial Maximum (LGM) (19–23 ka BP; Mix et al., 2001), the JS was almost isolated when the global sea level dropped by approximately 120 m; as a result, the JS was characterized by low salinity in surface water and anoxic deep water (Gorbarenko & Southon, 2000; Keigwin & Gorbarenko, 1992; Oba et al., 1991; Tada et al., 1999). The warmer $\text{U}^{37}\text{K}'$ -based sea surface temperature (SST) records, in

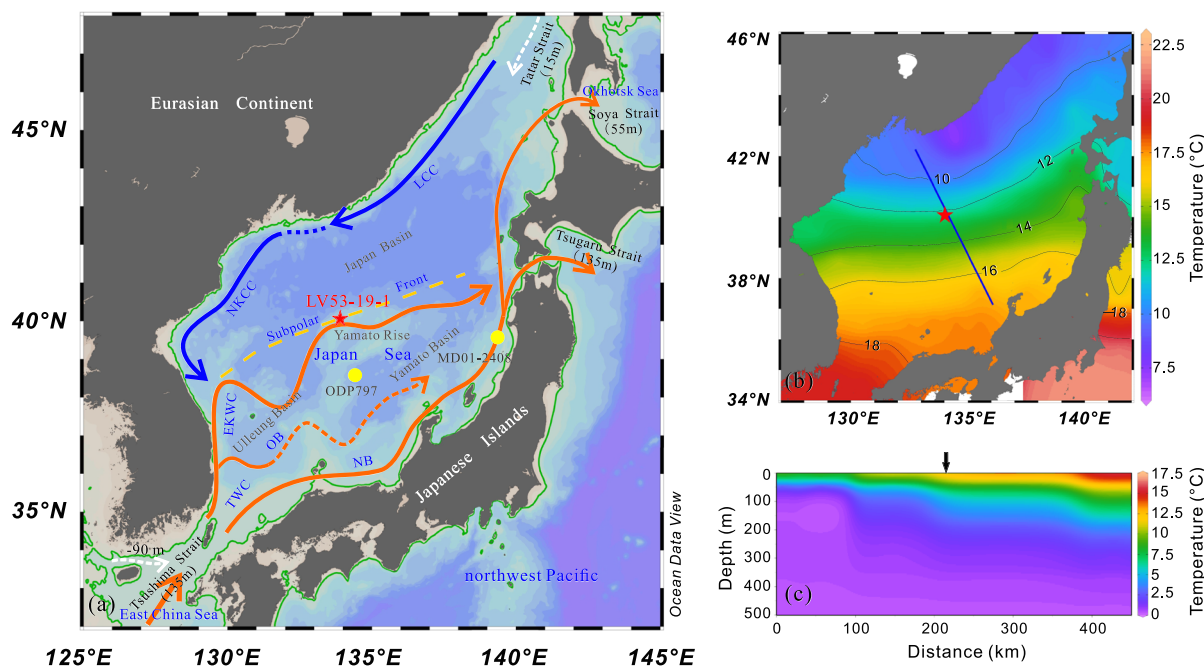


Figure 1. Core location and oceanographic setting of the JS. (a) Core location of LV53-19-1 (red star) and surface currents in the JS. Yellow dots: two cores used for comparison. Brown arrow lines: Tsushima Warm Current (TWC) with three branches; blue arrow lines: cold currents in northern part. Yellow dashed line: Subpolar Front (SPF) location. LCC: Liman Cold Current; NKCC: North Korea Cold Current; NB: nearshore branch of TWC; OB: Offshore Branch of TWC; EKWC: East Korea Warm Current. Green lines: 90-m water depth lines; white dashed arrow lines: possible freshwater inputs during last glacial period (Keigwin & Gorbarenko, 1992; Oba et al., 1991). (b) Annul mean surface SST from World Ocean Atlas 2013 (Locarnini et al., 2013). Blue line: transect across study site. (c) Annual mean temperature transect of upper 500 m. Black arrow: study site location.

comparison with the cold neighboring regions and/or modern conditions, were identified during LGM, but whether these reconstructed warmer SSTs represent the actual sea water thermal conditions in the period remains highly controversial (Fujine et al., 2006, 2009; Ishiwatari et al., 2001; Lee et al., 2008; Liu et al., 2014). Ishiwatari et al. (2001) interpreted the warm $U^{K'_{37}}$ -SSTs higher than those previously assumed during LGM by invoking a radiative equilibrium associated with the development of stable water stratification. Fujine et al. (2006) attributed the anomalously warm LGM temperatures, comparable to the SSTs during Holocene, to ecological or physiological influences on the alkenone proxy caused by low salinity.

Overall, the history of the upper water thermal structure in JS since the LGM remains equivocal, thus highlighting that it is beneficial to examine alternative, independent temperature proxies. Moreover, although of the complexity in the recording system by various proxies and likely conflicting results in temperature reconstructions, multitype proxies and their corroboration show different characteristics of upper ocean thermal structure. This is important for marginal seas sensitive to glacial-interglacial climate change in complex ways, for example, the JS, also giving the advantage using both TEX_{86} - and $U^{K'_{37}}$ -derived temperatures in this work.

Comparable to $U^{K'_{37}}$, another lipid proxy for temperature, TEX_{86} , is based on thaumarchaeota-produced isoprenoidal glycerol dialkyl glycerol tetraethers (GDGTs) and has been used successfully for water temperature reconstructions in different oceanic settings worldwide (Schouten et al., 2002; Schouten et al., 2013). Unfortunately, except for limited data on TEX_{86} temperature calibrations based on core top sediments (Kim et al., 2008, 2010; Seki et al., 2014) and one study on sinking particles (Park et al., 2019), no TEX_{86} -based temperature records have been reported in downcore sediments from the JS. In this study, we reconstructed the evolution of upper ocean temperatures and the related stratification in the central JS for the last 25 ka, based on paired downcore TEX_{86}^L - and $U^{K'_{37}}$ -derived sea water temperatures and the planktic foraminiferal $\delta^{18}\text{O}$ record.

2. Materials and Methods

2.1. Materials

A piston core LV53-19-1 (40.08°N, 133.97°E; 1,174-m water depth; 600-cm length) was collected from the northwest part of the Yamato Rise in the JS during the joint Chinese-Russian Cruise 53 with R/V “Akademik Lavrentyev,” in 2010. The core location is located at the boundary between the TWC and the cold water in the northern JS (Figure 1). The core was split and sampled in 2-cm intervals on board after recovery. The upper section with 125-cm length is used in this study. The lithology is characterized by laminated dark gray clayey silt from 125 to 78 cm (Figure S1 in the supporting information). Below, a laminated dark layer is separated by a light gray layer at 121–121.5 cm into two parts, corresponding to the thinly laminated layer 3 (TL3) and TL2 named after Tada et al. (1999). The section from 78 to 0 cm is mainly composed of light or dark gray bioturbated silt, except for the core top of 0–7 cm, especially 0–2 cm, where the sediment is brownish, indicating the modern sedimentary redox horizon. A total of 24 samples were taken for lipid analysis, with an average time resolution of 1.0 ka. In total, 33 samples were chosen for planktic foraminiferal oxygen isotope measurements.

2.2. Age Model

The age model was constructed based on seven accelerator mass spectrometry (AMS)¹⁴C radiocarbon dates. About 10 mg of either mixed planktic foraminifera or monospecific planktic foraminifera of *Globigerina bulloides* were picked from the >125-μm size fraction and measured at the National Ocean Sciences AMS Facility, Woods Hole Oceanographic Institution. The AMS¹⁴C ages were calibrated to calendar ages (“ka BP” hereafter) with the MARINE13 calibration curve (Reimer et al., 2013) and a local reservoir age of $\Delta R = 0$ year (Yokoyama et al., 2007). The calibration and age model were constructed using the software Bacon (Blaauw & Christen, 2011). The AMS¹⁴C and model ages (Table S1) indicate that sedimentation was continuous and free of turbidites in core LV53-19-1. The upper 125-cm sediment covers a record reaching back to ~25 ka BP (Figure S1a). The sedimentation rate ranges between 4.3 and 10.4 cm ka⁻¹ between 25.2 and 0.5 ka BP, except for low values of 1.1 to 2.2 cm ka⁻¹ during 13.7–7.8 ka BP (Figure S1b). The sedimentation rate is especially high in the upper 10 cm, which probably is caused by stretching of sediment during the process of sampling.

2.3. Lipid Analyses and Temperature Calibration

The lipid analyses were all carried out at Tongji University. The protocol for lipid extraction and fractionation follows references (Dong et al., 2015; Ge et al., 2014; Li et al., 2009; Wei et al., 2011) (Text S1), and the analysis and quantification for both lipids are described in detail in Text S2. The TEX₈₆ and U^{K'}₃₇ temperatures were reconstructed after Kim et al. (2010) and Müller et al. (1998), respectively; at the same time, in order to examine the influence of nonthermal factors on TEX₈₆ temperature estimates, the indices of Branched and Isoprenoid Tetraether (BIT) (Hopmans et al., 2004; Weijers et al., 2006) and ΔRI (Zhang et al., 2016) were also calculated (Text S3). By comparing with the modern data (Locarnini et al., 2013), the core top U^{K'}₃₇ temperature records SST in early summer, whereas TEX^L₈₆ records annual subsurface temperature (SubT) at 50 m (Text S4).

2.4. Planktic Foraminiferal δ¹⁸O Analysis

Planktic foraminiferal *G. bulloides* shells (30 shells, 250- to 300-μm size fraction) were measured for stable oxygen isotopes using a Finnigan-MAT 252 mass spectrometer at Tongji University. Precision was validated against a Chinese national carbonate standard (GBW04405) and NBS-19. Standard deviations were 0.07‰ for δ¹⁸O; all values are reported on the Pee Dee Belemnite (PDB) scale (Cheng et al., 2005).

3. Results and Discussion

3.1. Lipid and Foraminiferal δ¹⁸O Results

The most of proxies measured in the study show an evident change at the time of 16.3 ka BP (Figure S2 and Tables S2 and S3). The planktonic δ¹⁸O of foraminifera *G. bulloides* is light with an average value about 1.6‰ before 16.3 ka BP, but it increases quickly to 3.7‰ after 16.3 ka BP (Figure S2a). The alkenone content (C_{37:2} + C_{37:3}) is very low before 16.3 ka BP with a constant value about 10.6 ng g⁻¹ and gradually increases to a high level after 13.7 ka BP with the value higher than 100 ng g⁻¹ (Figure S2b). The U^{K'}₃₇-derived

temperature increases from 8.3°C at 24.7 ka BP to 15.1°C at 20.9 ka BP and then remains high value in general until 17.1 ka BP. It decreases quickly to 9.8°C at 16.3 ka BP and then increases generally to 17.1°C at 2.9 ka BP. The $U^{K'}$ ₃₇-derived temperature at 1 cm is 15.7°C (Figure S2c).

The GDGTs content of the six common isoprenoid GDGTs is high during periods of 24.7–16.3 ka BP and 13.7–8.7 ka BP, with an average higher than 1,000 ng g⁻¹ (Table S3 and Figure S2d). It is low at 15.9–14.1 ka BP and after 8.7 ka BP; the content of some compounds is lower than the detection limit in the top-most 7 cm of sediment (Figure S2d). Therefore, this uppermost part was excluded from the TEX_{86}^H temperature discussion. The variations in TEX_{86}^H - and TEX_{86}^L -derived temperatures reveal high values during last glacial, followed by a rapid decrease at 16.3 ka BP and subsequent low values until 8.7 ka BP, when they begin to increase again and reach another maximum at 2.9 ka BP (Figure S2f). The TEX_{86}^L -derived temperature is discussed in the below and also Text S4, and it is 5.9°C at the depth of 7–9 cm (0.3 ka BP). The BIT (Figure S2d) and ΔRI (Figure S2e) are both low in our record, with absolute values lower than the threshold of 0.3, implying that the estimation of TEX_{86}^L -based temperature should not be influenced by terrigenous GDGTs (Hopmans et al., 2004; Weijers et al., 2006) and other nontemperature factors (Zhang et al., 2016). Similar to the trends of TEX_{86}^L -derived temperatures, the ratio of GDGT-[2] to GDGT-[3] (hereafter GDGT-[2]/[3] ratio) is high during the period of 24.7–16.3 ka BP, with an average value of 12.4, and it decreases to less than 8.0 after 16.3 ka BP (Figure S2e).

In most areas of the modern ocean, Thaumarchaeota, as the primary GDGT producer of archaea, reach their maximum abundance near the base of the euphotic zone or in the epipelagic zone (50–200 m) and decrease toward the mesopelagic zone (Church et al., 2010; Dong et al., 2019; Mincer et al., 2007). As a result, TEX_{86} can be used as a temperature proxy for near-surface to shallow subsurface (<200 m) waters (Zhang & Liu, 2018). However, the community structure of Thaumarchaeota is apparently different along the water depth, with a “shallow cluster” in the epipelagic zone and “deep cluster” in the mesopelagic zone (Hu et al., 2011; Tolar et al., 2013; Villanueva et al., 2015). Correspondingly, there are potential links between the deep cluster of Thaumarchaeota with a high GDGT community structure index, GDGT-[2]/[3] ratio, and the shallow cluster with a low ratio (Villanueva et al., 2015). Dong et al. (2019) proposed to use the GDGT-[2]/[3] ratio as the indicator for the characterization of the Thaumarchaeota community or the paleo-productivity of the shallow cluster. Therefore, we use the GDGT-[2]/[3] ratio together with other proxies to better understand the ecological dynamics of the proxy carriers in relation to environmental changes. Based on our results, we divided the evolution of the upper water column into three different stages as follows (Figure 2).

3.2. Last Glacial Stage (24.7–16.3 Ka BP)

During this period, $U^{K'}$ ₃₇- and TEX_{86}^L -based temperatures were relatively high in contrast to the cold glacial SST in open seas around JS, for example, the northern East China Sea (Ijiri et al., 2005; Shi et al., 2014; Yamamoto et al., 2013) and the northwest Pacific (Sagawa et al., 2006); particularly, the TEX_{86}^L -record yields a maximum with an average of 15°C (Figure 2d). High LGM $U^{K'}$ ₃₇ temperatures have been previously reported in the JS and were either regarded as anomalous results caused directly by low salinities (Fujine et al., 2006; Fujine et al., 2009) or attributed to the radiative equilibrium associated with extremely increased upper ocean stratification (Ishiwatari et al., 2001), based on that significant upper ocean freshening (Keigwin & Gorbarenko, 1992; Oba et al., 1991). In addition, the alkenone content in the sediment is often very low, thus difficult to calculate $U^{K'}$ ₃₇ temperatures during the LGM (Lee et al., 2008; Liu et al., 2014). In this study, though the content of alkenones is low before 16.3 ka BP (Figure S2b), $U^{K'}$ ₃₇- and TEX_{86}^L -based temperatures are largely in agreement within calibration errors and change in the same direction, which makes it reasonable to assume that they represent the same water mass signals with the same depth and seasonality during the interval of 24.7–16.3 ka BP.

In our record, $\delta^{18}\text{O}$ values of *G. bulloides* are lighter from 24.7 to 16.3 ka BP, in contrast to the global $\delta^{18}\text{O}$ evolution (Figure 2b) (Lisiecki & Raymo, 2005). Similar phenomena of light $\delta^{18}\text{O}$ values in the JS were previously explained with less saline surface water (Gorbarenko et al., 1995, 2015; Kido et al., 2007; Kim et al., 2000; Oba et al., 1991; Yokoyama et al., 2007). When last glacial sea level was ~90 m lower than present, the JS was mostly isolated, and the inflow of the TWC was limited; coupled with continuous input of fresher water from surrounding rivers and excess precipitation over evaporation, the surface water became

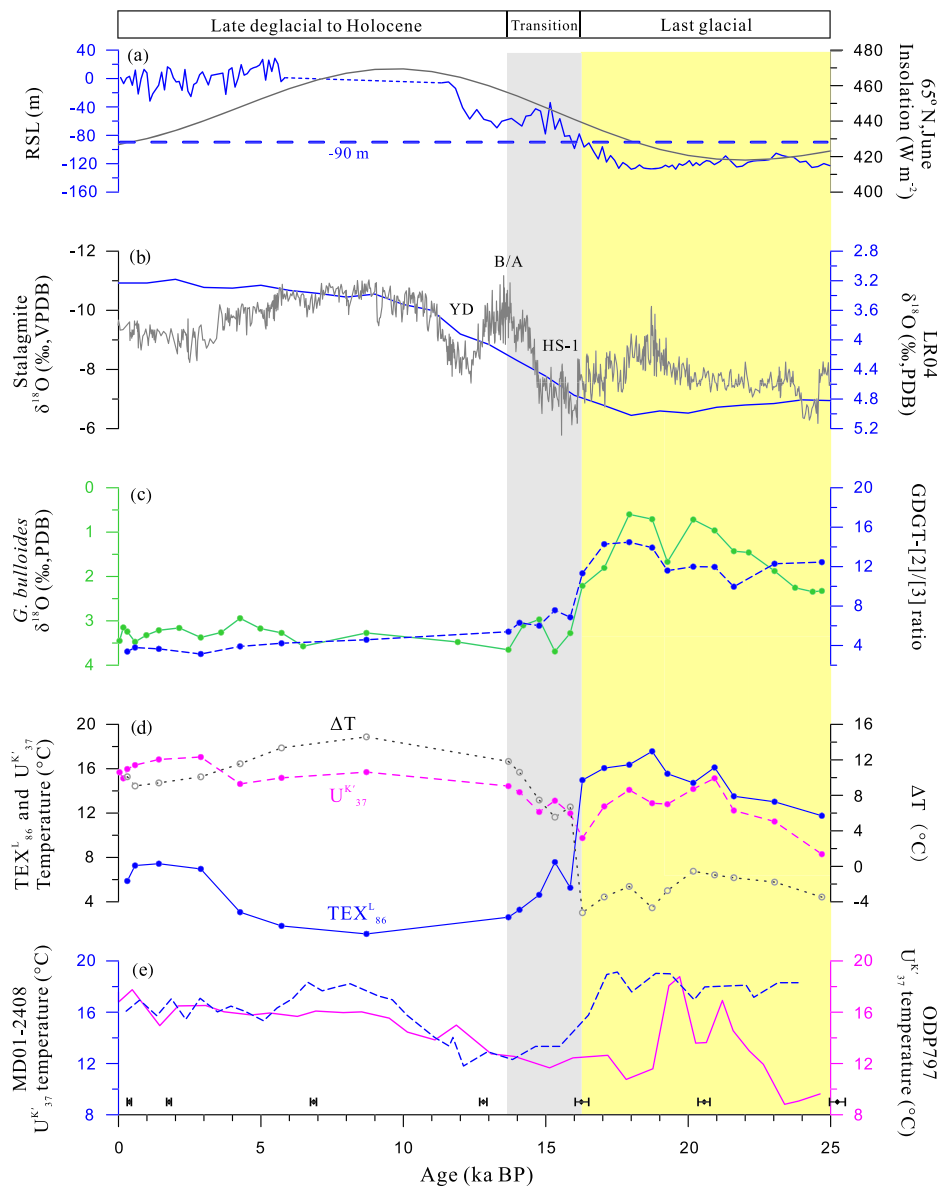


Figure 2. Comparison between results of LV53-19-1 (c, d) and other oceanic and climatic proxies. (a) Relative sea level (RSL) from Mediterranean Sea (Rohling et al., 2017); dashed line: -90 m sea level; gray: June summer insolation at 65°N (Berger, 1978). (b) $\delta^{18}\text{O}$ of Chinese stalagmite (blue line) (Cheng et al., 2016) and global $\delta^{18}\text{O}$ stack (gray line) (Lisiecki & Raymo, 2005). YD (Younger Dryas); B/A (Bølling/Allerød); HS-1 (Heinrich Stadial 1). (c) $\delta^{18}\text{O}$ of planktic foraminifera *G. bulloides* (green line) and GDGT-[2]/[3] ratio (blue dashed line). (d) $\text{U}^{K'}_{37}$ (pink dashed line) and TEX_{86}^L temperatures (blue line), plus difference between $\text{U}^{K'}_{37}$ and TEX_{86}^L temperatures (ΔT ; gray dotted line). (e) $\text{U}^{K'}_{37}$ temperatures of cores MD01-2408 (blue dashed line) (Fujine et al., 2009) and ODP797 (pink line) (Liu et al., 2014) from the JS. Yellow background: glacial to early deglacial stratified interval. Gray: deglacial transition to modern conditions. Bottom black bars in panel e: AMS ^{14}C ages with 2-sigma ranges.

fresher and the upper ocean thus more stratified (Keigwin & Gorbarenko, 1992; Oba & Irino, 2012; Tada et al., 1999; Xing et al., 2011). Between 24.7 and 16.3 ka BP, surface water and mixed layer conditions were largely different from the modern JS, which likely fostered a seasonal shift in timing of maximum alkenone production from early summer to summer because of the longer sea ice season caused by the weakening East Asian Summer Monsoon (EASM), as proposed for explaining high LGM $\text{U}^{K'}_{37}$ temperatures in the nearby northerly Okhotsk Sea (Harada et al., 2012; Seki et al., 2004). The seasonal shift in timing of haptophyte bloom to summer is also supported by the more similar trends and

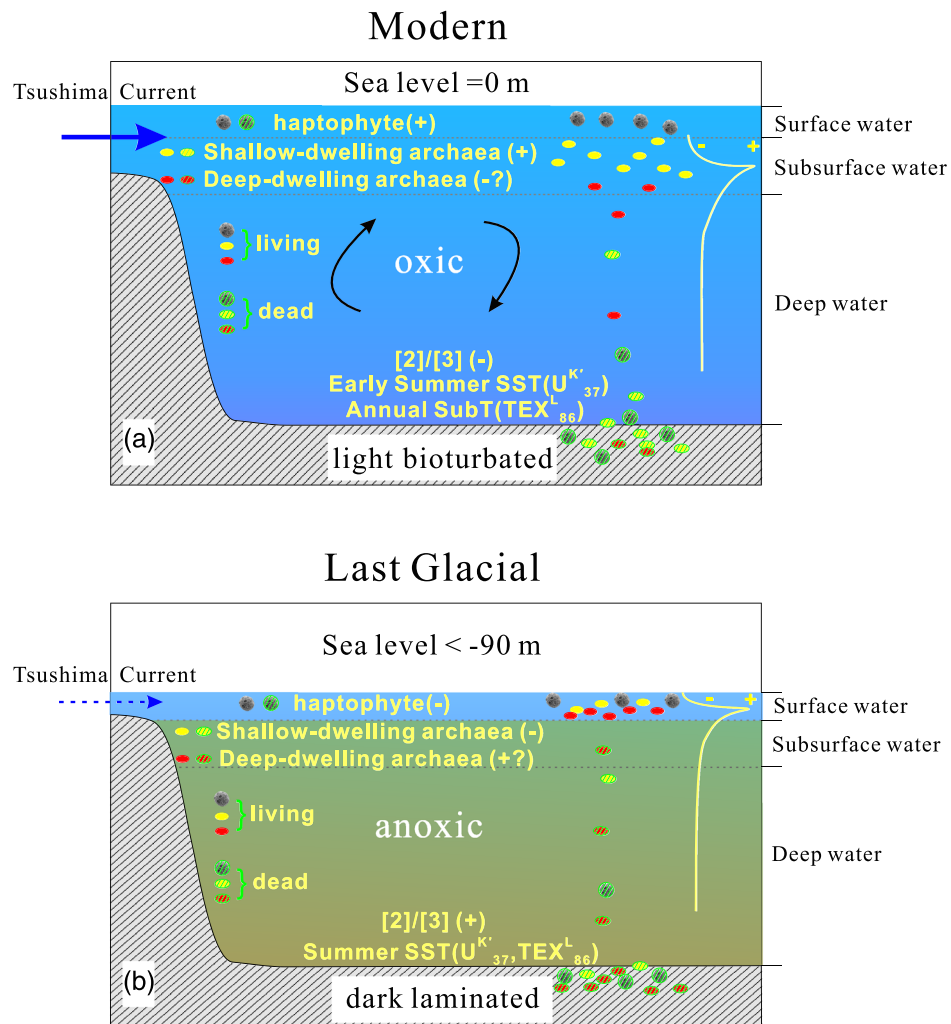


Figure 3. Schematic comparison of seasonality and habitat depth for biomarker production in surface and subsurface waters and their influence on both temperature proxies recorded in sediment between (a) modern and (b) last glacial setting, with approximately -90 m lower sea level, restricting water mass exchange with the open ocean. Yellow vertical curves indicate abundance of GDGT producer archaea in water column. Gray dashed lines illustrate different layers in upper water column.

correspondence of $U^{K'_{37}}$ temperature records, in our record and other two cores in the JS, with Chinese speleothem $\delta^{18}\text{O}$ data, as indicator of the EASM (Cheng et al., 2016), than after 16.3 ka BP (Figures 2d, 2e, and 2b).

Given that the TEX^L_{86} - and $U^{K'_{37}}$ -based temperature records run largely parallel and are in agreement within calibration errors, we assume that the TEX^L_{86} -based temperature also reflects the summer SST during 24.7–16.3 ka BP, rather than SubT like at present. We hypothesize this change being caused as follows (Figure 3).

Thaumarchaeota are abundant in surface water at high latitudes and polar oceans (Tolar et al., 2013, and references therein). In the Okhotsk Sea, Bering Sea, and northwest Pacific, the TEX^L_{86} -based temperature is usually interpreted as a shallow water temperature (i.e., about 20 m) in summer (Lattaud et al., 2018; Meyer et al., 2016; Seki et al., 2009, 2014). When the upper ocean becomes stratified in summer, temperature maxima are restricted to the shallow surface water. Ammonium concentrations peak in the similar depth interval at the same time; because Thaumarchaeota are ammonia-oxidizing chemoautotrophs, their maximum abundances will accumulate in that identical depth over summer (Seki et al., 2014). During glacial

sea level lowstands of lower than -125 to -90 m around 24.7 – 16.3 ka BP (Rohling et al., 2017), the JS was nearly isolated from neighboring oceanic regions (Figure 3b). As a result, surface waters became fresher and the upper ocean strongly stratified, which is supported by our light *G. bulloides* $\delta^{18}\text{O}$ values (Figure 2b), low alkenone contents (Figure S2b), and the occurrence of laminated sediments (Figure S1b). In essence, the oceanographic characteristics of the glacial stratified JS were more comparable to modern subpolar settings, like in the modern Okhotsk Sea or Bering Sea. Thus, we presume the maximum Thaumarchaeota production shifted into the summer surface or mixed layer water in the JS (Figure 3b). In addition, the deep-dwelling archaea may have shoaled their habitat depth to surface waters because the oxygen-depleted subsurface or deep water conditions were no longer suitable for survival. Such a shallower habitat depth of deep-dwelling archaea makes the associated high-[2]/[3]-ratio GDGT easier to export to the sediment in large sinking aggregates or fecal pellets than from a deep habitat depth (Wuchter et al., 2006). At the same time, the productivity of shallow-dwelling archaea decreased because of the thinned mixed layer caused by strong stratification.

As a result, the increasing GDGT contribution of deep-dwelling archaea and decreasing contribution of the shallow dwelling led to high GDGT-[2]/[3] ratios in the sediment (Figure 3b). We propose that the high glacial GDGT-[2]/[3] ratio (>10) can be used as an indicator for strongly stratified upper ocean during the low sea level (<-90 m) period, when the JS was characterized by relatively high and similar $\text{U}^{\text{K}'}_{37}$ - and $\text{TEX}^{\text{L}}_{86}$ -based summer SST.

3.3. Deglacial Transition Stage (16.3–13.7 Ka BP)

The most prominent feature in our record is the diverging two proxy-based temperature records between 16.3 and 13.7 ka BP. The continuous increase in the $\text{U}^{\text{K}'}_{37}$ -SST from 9.8°C to 14.4°C in this period is accompanied by a simultaneous but sudden decrease in $\text{TEX}^{\text{L}}_{86}$ temperatures from 15.0°C to 2.6°C , dropping 9.7°C within only a few hundred years or less between 16.3 and 15.9 ka BP (Figure 2d). In this interval, the difference between $\text{U}^{\text{K}'}_{37}$ -SST and $\text{TEX}^{\text{L}}_{86}$ -derived temperature (ΔT) increases from -5°C to 12°C (Figure 2d).

This episode corresponds to the deglacial interval with a rapid relative sea level rise from ~-90 to ~-40 m (Rohling et al., 2017) (Figure 2a). Our data imply that the upper ocean stratification of the JS began to quickly collapse when the sea level rose above -90 m, opening and connecting the basin to the adjacent seas again (Keigwin & Gorbarenko, 1992; Oba et al., 1991). As a result, relatively saline water flowed into the JS through the Tsugaru Strait (Ikeda et al., 1999; Isobe, 2020; Oba et al., 1991) and/or Tsushima Strait (Domitus & Oda, 2006; Keigwin & Gorbarenko, 1992). Increased salinity and strengthened convection resulted in the significant increase in planktic foraminiferal $\delta^{18}\text{O}$ values (Figure 2c) and the alkenone content (Figure S2b). Accordingly, the sediment changed from a dark laminated to light bioturbated or homogeneous facies (Figure S1b), indicating that the deep water conditions changed from anoxic to oxic at that time.

We invoke the shift in seasonality, maximum archaea production depth, and archaeal community structure to explain the sharp decrease in $\text{TEX}^{\text{L}}_{86}$ temperatures and the GDGT-[2]/[3] ratio (Figures 2d and 2c). During the period, the surface conditions in JS changed from the last glacial mode to modern regime (Figure 3a). When the upper ocean stratification became weaker and deep water increasingly oxygenated along with the increase in the SST indicated by $\text{U}^{\text{K}'}_{37}$ temperatures, the seasonality and maximum abundance depth of Thaumarchaeota production shifted from summer surface water to the annual subsurface, notably quicker than the change in other proxies, thus resulting in a sudden decrease of $\text{TEX}^{\text{L}}_{86}$ temperatures. Likely, this distinct pattern provides evidence for a nonlinear threshold-like change in either the optimal habitat of Thaumarchaeota or the stratification, and by inference oxygenation conditions, to increased interbasin water mass exchange due to sea level rise. At the same time, the contribution of shallow-dwelling archaea increased and caused a decrease in GDGT-[2]/[3] ratios. Similarly, we propose a seasonality shift of the $\text{U}^{\text{K}'}_{37}$ -SST signal from glacial summer to interglacial early summer. The increasing trend of $\text{U}^{\text{K}'}_{37}$ -SST implies that a strong influence of the EASM on SSTs overcame the negative seasonal impact from summer to early summer during the period (Figures 2d and 2b). Therefore, during the deglacial transition, the divergence between two proxy-based temperature records mainly represents the increasing difference between a warming temperature, influenced by enhanced EASM, from summer to early summer SST recorded by haptophyte and cooling temperature variations from summer SST to annual subT recorded by archaea.

In our records, the transition from an extremely cold HS-1 to a warm B/A interval is not evident like in other records from the JS (e.g., as shown in Figure 2e). This is likely due to the observed reconnection of the JS to oceanic water masses through newly submerged gateways and rapid change in the basin's water mass structure, which superseded the effects of hemispheric and regional temperature changes across these deglacial millennial-scale events, which were recorded in several locations in the open ocean east of Japan (Sagawa et al., 2006; Sagawa & Ikehara, 2008).

3.4. Late Deglacial to Holocene (13.7 ka BP to Present Day)

The main characteristic of this interval is the large divergence between our two temperature records (Figure 2d). Most of our data during this period remain relatively constant and similar to present-day values, indicating relatively stable long-term upper ocean Holocene conditions. Especially the constant, low GDGT-[2]/[3] ratio indicates that the depth and seasonality for the GDGT producers remains similar across this phase, that is, our TEX^L_{86} temperatures likely represent annual mean SubT at 50 m, while the $\text{U}^{K'}_{37}$ temperatures reflect early summer SST (Figure 3a).

During this interval, ΔT can be used to indicate the thermal gradient between surface and subsurface water. The ΔT is 14.6°C at 8.7 ka BP and decreased to 9.1°C at 0.6 ka BP (Figure 2d). At the same time, the TEX^L_{86} -SubT continuously increased during the period of 8.7–0.6 ka BP. In the modern JS, the TWC plays an important role in the upper ocean circulation. The TWC water occupy the upper 150 m in the south (Chang et al., 2004), and its influence declines northward to the central part of the Subpolar Front area with decreasing penetration depth (Figures 1b and 1c). Therefore, the decrease in ΔT and increase in TEX^L_{86} -SubT likely reflects the strengthening influence of TWC in our study area. Our data indicate that the TWC flowed into JS after ~8.7 ka BP, in line with earlier studies in the JS (Domitsu & Oda, 2008; Itaki et al., 2004; Takei et al., 2002; Zou et al., 2012) and in the East China Sea (Jian et al., 2000; Li et al., 2007).

Both our measurements of $\text{U}^{K'}_{37}$ -SST and two other SST records in the JS (Figures 2d and 2e) show similar SST variations, correlating in their trends with the EASM between 13.7 BP and 4.3 ka BP (Figure 2b), suggesting a dominant control of the EASM on surface water temperatures and stratification. In addition, though the EASM weakened after 4.3 ka BP, our $\text{U}^{K'}_{37}$ record maintains relatively high SSTs, which implies an increasing influence of TWC water and less EASM influence on the regional SST characteristics during the middle to late Holocene.

4. Conclusions

We reconstructed the evolution of upper-ocean stratification based on paired $\text{U}^{K'}_{37}$ and TEX^L_{86} sea water temperatures from the central JS. Between 24.7 and 16.3 ka BP, similar $\text{U}^{K'}_{37}$ and TEX^L_{86} -derived summer SSTs indicate fresher surface water and a more stratified upper ocean. A deglacial transition in the upper water column structure occurred based on diverging $\text{U}^{K'}_{37}$ - and TEX^L_{86} -derived temperatures, as well as other proxies such as planktic foraminiferal $\delta^{18}\text{O}$ values and GDGT-[2]/[3] ratios between 16.3 and 13.7 ka BP. The stratification was weak, and the upper water condition was mostly similar to present-day conditions after 13.7 ka BP. While the difference between $\text{U}^{K'}_{37}$ -SST and TEX^L_{86} -SubT was large during 13.7–8.7 ka BP, it thereafter decreased until 0.6 ka BP, which indicates TWC inflow to the JS after ~8.7 ka BP.

Our results suggest that high LGM $\text{U}^{K'}_{37}$ -SST in the JS in general reflects the seasonal shift in the timing of haptophyte blooms. We propose that the high value of GDGT-[2]/[3] ratio (larger than 10) can be used as an indicator to identify these fresher and more stratified upper ocean conditions during low sea level intervals.

Data Availability Statement

All data are included in the supporting information and available the PANGAEA data repository (<https://doi.pangaea.de/10.1594/PANGAEA.920797>).

References

- Berger, A. (1978). Long-term variations of daily insolation and Quaternary climatic changes. *Journal of the Atmospheric Sciences*, 35(12), 2362–2367. [https://doi.org/10.1175/1520-0469\(1978\)035%3C2362:LTVODI%3E2.0.CO;2](https://doi.org/10.1175/1520-0469(1978)035%3C2362:LTVODI%3E2.0.CO;2)
- Blaauw, M., & Christen, J. A. (2011). Flexible paleoclimate age-depth models using an autoregressive gamma process. *Bayesian Analysis*, 6(3), 457–474.

Acknowledgments

The authors kindly thank Chuanlun Zhang, Li Li, and Xinrong Cheng for laboratory analysis, Hui Wang and Jiangtao Zhao for laboratory assistance, and Liang Dong, Huangmin Ge, Yue Wang, Shuzhuang Wu, and Junjie Wu for data discussion. This study is supported by China NSFC grants (U1606401 and 41420104005), National Program on Global Change and Air-Sea Interaction (GASI-GEOGE-03 and GASI-GEOGE-04), German BMBF grants (NOPAWAC, 03F0785A, and PalMod, 01LP1504A), AWI institutional funds PACES-II, and the Taishan Scholar Program of Shandong.

- Chang, K. I., Teague, W. J., Lyu, S. J., Perkins, H. T., Lee, D. K., Watts, D. R., et al. (2004). Circulation and currents in the southwestern East/Japan Sea: Overview and review. *Progress in Oceanography*, 61(2–4), 105–156. <https://doi.org/10.1016/j.pocean.2004.06.005>
- Cheng, H., Edwards, R. L., Sinha, A., Spötl, C., Yi, L., Chen, S., et al. (2016). The Asian monsoon over the past 640,000 years and ice age terminations. *Nature*, 534(7609), 640–646. <https://doi.org/10.1038/nature18591>
- Cheng, X., Huang, B., Jian, Z., Zhao, Q., Tian, J., & Li, J. (2005). Foraminiferal isotopic evidence for monsoonal activity in the South China Sea: A present-LGM comparison. *Marine Micropaleontology*, 54(1–2), 125–139. <https://doi.org/10.1016/j.marmicro.2004.09.007>
- Church, M. J., Wai, B., Karl, D. M., & Delong, E. F. (2010). Abundances of crenarchaeal amoA genes and transcripts in the Pacific Ocean. *Environmental Microbiology*, 12(3), 679–688. <https://doi.org/10.1111/j.1462-2920.2009.02108.x>
- Domitus, H., & Oda, M. (2006). Linkages between surface and deep circulations in the southern Japan Sea during the last 27,000 years: Evidence from planktic foraminiferal assemblages and stable isotope records. *Marine Micropaleontology*, 61(4), 155–170. <https://doi.org/10.1016/j.marmicro.2006.06.006>
- Domitus, H., & Oda, M. (2008). Holocene influx of the Tsushima Current into the Japan Sea signalled by spatial and temporal changes in *Neogloboquadrina incompata* distribution. *The Holocene*, 18(2), 345–352. <https://doi.org/10.1177/0959683607086772>
- Dong, L., Li, Q., Li, L., & Zhang, C. L. (2015). Glacial-interglacial contrast in MBT/CBT proxies in the South China Sea: Implications for marine production of branched GDGTs and continental teleconnection. *Organic Geochemistry*, 79, 74–82. <https://doi.org/10.1016/j.orggeochem.2014.12.008>
- Dong, L., Li, Z., & Jia, G. (2019). Archaeal ammonia oxidation plays a part in late Quaternary nitrogen cycling in the South China Sea. *Earth and Planetary Science Letters*, 509, 38–46. <https://doi.org/10.1016/j.epsl.2018.12.023>
- Fujine, K., Tada, R., & Yamamoto, M. (2009). Paleotemperature response to monsoon activity in the Japan Sea during the last 160 kyr. *Palaeogeography, Palaeoclimatology, Palaeoecology*, 280(3–4), 350–360. <https://doi.org/10.1016/j.palaeo.2009.06.022>
- Fujine, K., Yamamoto, M., Tada, R., & Kido, Y. (2006). A salinity-related occurrence of a novel alkenone and alkenoate in Late Pleistocene sediments from the Japan Sea. *Organic Geochemistry*, 37(9), 1074–1084. <https://doi.org/10.1016/j.orggeochem.2006.05.004>
- Gamo, T. (1999). Global warming may have slowed down the deep conveyor belt of a marginal sea of the northwestern Pacific: Japan Sea. *Geophysical Research Letters*, 26(20), 3137–3140. <https://doi.org/10.1029/1999GL002341>
- Ge, H., Zhang, C. L., Li, J., Versteegh, G. J., Hu, B., Zhao, J., & Dong, L. (2014). Tetraether lipids from the southern Yellow Sea of China: Implications for the variability of East Asia Winter Monsoon in the Holocene. *Organic Geochemistry*, 70, 10–19. <https://doi.org/10.1016/j.orggeochem.2014.02.011>
- Gorbarenko, S., Shi, X., Rybiakova, Y., Bosin, A., Malakhov, M., Zou, J., et al. (2015). Fine structure of dark layers in the central Japan Sea and their relationship with the abrupt climate and sea level changes over the last 75 ka inferred from lithophysical, geochemical and pollen results. *Journal of Asian Earth Sciences*, 114, 476–487. <https://doi.org/10.1016/j.jseas.2015.04.040>
- Gorbarenko, S., & Sounthor, J. (2000). Detailed Japan Sea paleoceanography during the last 25 kyr: Constraints from AMS dating and $\delta^{18}\text{O}$ of planktonic foraminifera. *Palaeogeography, Palaeoclimatology, Palaeoecology*, 156(3–4), 177–193. [https://doi.org/10.1016/S0031-0182\(99\)00137-6](https://doi.org/10.1016/S0031-0182(99)00137-6)
- Gorbarenko, S. A., Pliss, S. G., Sounthor, J. R., Kashgarian, M., Verkhovskaya, N. B., & Kundyshev, A. S. (1995). Detailed carbonate stratigraphy of the Japan Sea sediments during last glaciation-Holocene. *Terrestrial, Atmospheric and Oceanic Sciences*, 6(1), 103–113. [https://doi.org/10.3319/TAO.1995.6.1.103\(KEEP-MASS\)](https://doi.org/10.3319/TAO.1995.6.1.103(KEEP-MASS))
- Harada, N., Sato, M., Seki, O., Timmermann, A., Moosse, H., Bendle, J., et al. (2012). Sea surface temperature changes in the Okhotsk Sea and adjacent North Pacific during the last glacial maximum and deglaciation. *Deep Sea Research Part II: Topical Studies in Oceanography*, 61–64, 93–105. <https://doi.org/10.1016/j.dsr2.2011.12.007>
- Hopmans, E. C., Weijers, J. W., Schefuß, E., Herfort, L., Damsté, J. S. S., & Schouten, S. (2004). A novel proxy for terrestrial organic matter in sediments based on branched and isoprenoid tetraether lipids. *Earth and Planetary Science Letters*, 224(1–2), 107–116. <https://doi.org/10.1016/j.epsl.2004.05.012>
- Hu, A., Jiao, N., & Zhang, C. L. (2011). Community structure and function of planktonic Crenarchaeota: Changes with depth in the South China Sea. *Microbial Ecology*, 62(3), 549–563. <https://doi.org/10.1007/s00248-011-9866-z>
- Ijiri, A., Wang, L., Oba, T., Kawahata, H., Huang, C.-Y., & Huang, C.-Y. (2005). Paleoenvironmental changes in the northern area of the East China Sea during the past 42,000 years. *Palaeogeography, Palaeoclimatology, Palaeoecology*, 219(3–4), 239–261. <https://doi.org/10.1016/j.palaeo.2004.12.028>
- Ikeda, M., Suzuki, F., & Oba, T. (1999). A box model of glacial-interglacial variability in the Japan Sea. *Journal of Oceanography*, 55(4), 483–492. <https://doi.org/10.1023/A:1007831122343>
- Ikehara, K. (2003). Late Quaternary seasonal sea-ice history of the northeastern Japan Sea. *Journal of Oceanography*, 59(5), 585–593. <https://doi.org/10.1023/B:JOCE.0000009588.49944.3d>
- Ikehara, K., & Itaki, T. (2007). Millennial-scale fluctuations in seasonal sea-ice and deep-water formation in the Japan Sea during the late Quaternary. *Palaeogeography, Palaeoclimatology, Palaeoecology*, 247(1–2), 131–143. <https://doi.org/10.1016/j.palaeo.2006.11.026>
- Ishiwatari, R., Houtatsu, M., & Okada, H. (2001). Alkenone-sea surface temperatures in the Japan Sea over the past 36 kyr: Warm temperatures at the last glacial maximum. *Organic Geochemistry*, 32(1), 57–67. [https://doi.org/10.1016/S0146-6380\(00\)00151-0](https://doi.org/10.1016/S0146-6380(00)00151-0)
- Isobe, A. (2020). Paleo-ocean destratification triggered by the subduction of the Oyashio water into the Sea of Japan after the Last Glacial Maximum. *Paleoceanography and Paleoclimatology*, 7(4). <https://doi.org/10.1029/2019EA000582>
- Itaki, T., Ikehara, K., Motoyama, I., & Hasegawa, S. (2004). Abrupt ventilation changes in the Japan Sea over the last 30 ky: Evidence from deep-dwelling radiolarians. *Palaeogeography, Palaeoclimatology, Palaeoecology*, 208(3–4), 263–278. <https://doi.org/10.1016/j.palaeo.2004.03.010>
- Jian, Z., Wang, P., Saito, Y., Wang, J., Pflaumann, U., Oba, T., & Cheng, X. (2000). Holocene variability of the Kuroshio current in the Okinawa Trough, northwestern Pacific Ocean. *Earth and Planetary Science Letters*, 184(1), 305–319. [https://doi.org/10.1016/S0012-821X\(00\)00321-6](https://doi.org/10.1016/S0012-821X(00)00321-6)
- Keigwin, L., & Gorbarenko, S. (1992). Sea level, surface salinity of the Japan Sea, and the Younger Dryas event in the northwestern Pacific Ocean. *Quaternary Research*, 37(3), 346–360. [https://doi.org/10.1016/0033-5894\(92\)90072-Q](https://doi.org/10.1016/0033-5894(92)90072-Q)
- Kido, Y., Minami, I., Tada, R., Fujine, K., Irino, T., Ikehara, K., & Chun, J.-H. (2007). Orbital-scale stratigraphy and high-resolution analysis of biogenic components and deep-water oxygenation conditions in the Japan Sea during the last 640 kyr. *Palaeogeography, Palaeoclimatology, Palaeoecology*, 247(1–2), 32–49. <https://doi.org/10.1016/j.palaeo.2006.11.020>
- Kim, J.-H., Schouten, S., Hopmans, E. C., Donner, B., & Simmingsie Damsté, J. S. (2008). Global sediment core-top calibration of the TEX₈₆ paleothermometer in the ocean. *Geochimica et Cosmochimica Acta*, 72(4), 1154–1173. <https://doi.org/10.1016/j.gca.2007.12.010>

- Kim, J.-H., van der Meer, J., Schouten, S., Helmke, P., Willmott, V., Sangiorgi, F., et al. (2010). New indices and calibrations derived from the distribution of crenarchaeal isoprenoid tetraether lipids: Implications for past sea surface temperature reconstructions. *Geochimica et Cosmochimica Acta*, 74(16), 4639–4654. <https://doi.org/10.1016/j.gca.2010.05.027>
- Kim, J. M., Kennett, J. P., Park, B. K., Kim, D. C., Kim, G. Y., & Roark, E. B. (2000). Paleoceanographic change during the last deglaciation, East Sea of Korea. *Paleoceanography*, 15(2), 254–266. <https://doi.org/10.1029/1999PA000393>
- Lattaud, J., Lo, L., Huang, J. J., Chou, Y. M., Gorbarenko, S. A., Sinninghe Damsté, J. S., & Schouten, S. (2018). A comparison of late Quaternary organic proxy-based paleotemperature records of the central Sea of Okhotsk. *Paleoceanography and Paleoclimatology*, 33(7), 732–744. <https://doi.org/10.1029/2018PA003388>
- Lee, K. E., Bahk, J. J., & Choi, J. (2008). Alkenone temperature estimates for the East Sea during the last 190,000 years. *Organic Geochemistry*, 39(6), 741–753. <https://doi.org/10.1016/j.orggeochem.2008.02.003>
- Li, L., Wang, H., Li, J., Zhao, M., & Wang, P. (2009). Changes in sea surface temperature in western South China Sea over the past 450 ka. *Chinese Science Bulletin*, 54(18), 3335–3343. <https://doi.org/10.1007/s11434-009-0083-9>
- Li, T., Sun, R., Zhang, D., Liu, Z., Li, Q., & Jiang, B. (2007). Evolution and variation of the Tsushima warm current during the late Quaternary: Evidence from planktonic foraminifera, oxygen and carbon isotopes. *Science in China Series D: Earth Sciences*, 50(5), 725–735. <https://doi.org/10.1007/s11430-007-0003-2>
- Lisiecki, L. E., & Raymo, M. E. (2005). A Pliocene-Pleistocene stack of 57 globally distributed benthic $\delta^{18}\text{O}$ records. *Paleoceanography*, 20, PA1003. <https://doi.org/10.1029/2004PA001071>
- Liu, Y. G., Chen, J. J., Chen, J. X., Xing, L., Zou, J. J., & Yao, Z. Q. (2014). Variations of alkenone temperature in the Sea of Japan during the last 170 ka and its paleoceanographic implications. *Chinese Science Bulletin*, 59(33), 4498–4509. <https://doi.org/10.1007/s11434-014-0367-6>
- Locarnini, R. A., Mishonov, A. V., Antonov, J. I., Boyer, T. P., Garcia, H. E., Baranova, O. K., et al. (2013). World Ocean Atlas 2013, Volume 1: Temperature. In S. Levitus (Eds.), *NOAA Atlas NESDIS* (Vol. 73, p. 40). Washington, DC: U.S. Government Printing Office.
- Lohmann, G., Lembeke-Jene, L., Tiedemann, R., Gong, X., Scholz, P., Zou, J., & Shi, X. (2019). Challenges in the paleoclimatic evolution of the Arctic and subarctic Pacific since the last glacial period—The Sino-German Pacific-Arctic Experiment (SiGePAX). *Challenges*, 10(1), 13. <https://doi.org/10.3390/challe10010013>
- Meyer, V. D., Max, L., Heftet, J., Tiedemann, R., & Mollenhauer, G. (2016). Glacial-to-Holocene evolution of sea surface temperature and surface circulation in the subarctic northwest Pacific and the Western Bering Sea. *Paleoceanography*, 31, 916–927. <https://doi.org/10.1002/2015PA002877>
- Mincer, T. J., Church, M. J., Taylor, L. T., Preston, C., Karl, D. M., & DeLong, E. F. (2007). Quantitative distribution of presumptive archaeal and bacterial nitrifiers in Monterey Bay and the North Pacific Subtropical Gyre. *Environmental Microbiology*, 9(5), 1162–1175. <https://doi.org/10.1111/j.1462-2920.2007.01239.x>
- Mix, A. C., Bard, E., & Schneider, R. R. (2001). Environmental processes of the ice age: Land, oceans, glaciers (EPILOG). *Quaternary Science Reviews*, 20(4), 627–657. [https://doi.org/10.1016/S0277-3791\(00\)00145-1](https://doi.org/10.1016/S0277-3791(00)00145-1)
- Müller, P. J., Kirst, G., Ruhland, G., Von Storch, I., & Rosell-Melé, A. (1998). Calibration of the alkenone paleotemperature index $U^{K'_{37}}$ based on core-top from the eastern South Atlantic and the global ocean (60°N - 60°S). *Geochimica et Cosmochimica Acta*, 62(10), 1757–1772. [https://doi.org/10.1016/S0016-7037\(98\)00097-0](https://doi.org/10.1016/S0016-7037(98)00097-0)
- Oba, T., & Irino, T. (2012). Sea level at the last glacial maximum, constrained by oxygen isotopic curves of planktonic foraminifera in the Japan Sea. *Journal of Quaternary Science*, 27(9), 941–947. <https://doi.org/10.1002/jqs.2585>
- Oba, T., Kato, M., Kitazato, H., Koizumi, I., Omura, A., Sakai, T., & Takayama, T. (1991). Paleoenvironmental changes in the Japan Sea during the last 85,000 years. *Paleoceanography*, 6(4), 499–518. <https://doi.org/10.1029/91PA00560>
- Park, Y.-H., Kim, H. J., Son, J. W., Yoo, C. M., & Khim, B.-K. (2019). Biomarker-based seawater temperatures of winter sinking particles and core-top sediment in the Ulleung Basin of the East Sea. *Ocean Science Journal*, 54(3), 487–495. <https://doi.org/10.1007/s12601-019-0017-7>
- Reimer, P. J., Bard, E., Bayliss, A., Beck, J. W., Blackwell, P. G., Ramsey, C. B., et al. (2013). IntCal13 and Marine13 radiocarbon age calibration curves 0–50,000 years cal BP. *Radiocarbon*, 55(4), 1869–1887. https://doi.org/10.2458/azu_js_rc.55.16947
- Rohling, E. J., Hibbert, F. D., Williams, F. H., Grant, K. M., Marino, G., Foster, G. L., et al. (2017). Differences between the last two glacial maxima and implications for ice-sheet, $\delta^{18}\text{O}$, and sea-level reconstructions. *Quaternary Science Reviews*, 176, 1–28. <https://doi.org/10.1016/j.quascirev.2017.09.009>
- Sagawa, T., & Ikebara, K. (2008). Intermediate water ventilation change in the subarctic northwest Pacific during the last deglaciation. *Geophysical Research Letters*, 35, L24702. <https://doi.org/10.1029/2008GL035133>
- Sagawa, T., Toyoda, K., & Oba, T. (2006). Sea surface temperature record off central Japan since the Last Glacial Maximum using planktonic foraminiferal Mg/Ca thermometry. *Journal of Quaternary Science*, 21(1), 63–73. <https://doi.org/10.1002/jqs.941>
- Schouten, S., Hopmans, E. C., & Damste, J. S. S. (2013). The organic geochemistry of glycerol dialkyl glycerol tetraether lipids: A review. *Organic Geochemistry*, 54, 19–61. <https://doi.org/10.1016/j.orggeochem.2012.09.006>
- Schouten, S., Hopmans, E. C., Schefuß, E., & Sinninghe Damsté, J. S. (2002). Distributional variations in marine crenarchaeotal membrane lipids: A new tool for reconstructing ancient sea water temperatures? *Earth and Planetary Science Letters*, 204(1-2), 265–274. [https://doi.org/10.1016/S0012-821X\(02\)00979-2](https://doi.org/10.1016/S0012-821X(02)00979-2)
- Seki, O., Bendle, J. A., Harada, N., Kobayashi, M., Sawada, K., Moosse, H., et al. (2014). Assessment and calibration of TEX₈₆ paleothermometry in the Sea of Okhotsk and sub-polar North Pacific region: Implications for paleoceanography. *Progress in Oceanography*, 126, 254–266. <https://doi.org/10.1016/j.pocean.2014.04.013>
- Seki, O., Kawamura, K., Ikebara, M., Nakatsuka, T., & Oba, T. (2004). Variation of alkenone sea surface temperature in the Sea of Okhotsk over the last 85 kyrs. *Organic Geochemistry*, 35(3), 347–354. <https://doi.org/10.1016/j.orggeochem.2003.10.011>
- Seki, O., Sakamoto, T., Sakai, S., Schouten, S., Hopmans, E. C., Sinninghe Damste, J. S., & Pancost, R. D. (2009). Large changes in seasonal sea ice distribution and productivity in the Sea of Okhotsk during the deglaciations. *Geochimica, Geophysics, Geosystems*, 10, Q10007. <https://doi.org/10.1029/2009GC002613>
- Shi, X., Wu, Y., Zou, J., Liu, Y., Ge, S., Zhao, M., et al. (2014). Multiproxy reconstruction for Kuroshio responses to northern hemispheric oceanic climate and the Asian Monsoon since Marine Isotope Stage 5.1 (~ 88 ka). *Climate of the Past*, 10(5), 1735–1750. <https://doi.org/10.5194/cp-10-1735-2014>
- Tada, R., Irino, T., & Koizumi, I. (1999). Land-ocean linkages over orbital and millennial timescales recorded in Late Quaternary sediments of the Japan Sea. *Paleoceanography*, 14(2), 236–247. <https://doi.org/10.1029/1998PA900016>
- Takei, T., Minoura, K., Tsukawaki, S., & Nakamura, T. (2002). Intrusion of a branch of the Oyashio Current into the Japan Sea during the Holocene. *Paleoceanography*, 17(3), 1039. <https://doi.org/10.1029/2001PA000666>

- Tolar, B. B., King, G. M., & Hollibaugh, J. T. (2013). An analysis of Thaumarchaeota populations from the northern Gulf of Mexico. *Frontiers in Microbiology*, 4, 72. <https://doi.org/10.3389/fmicb.2013.00072>
- Villanueva, L., Schouten, S., & Sinninghe Damsté, J. S. (2015). Depth-related distribution of a key gene of the tetraether lipid biosynthetic pathway in marine T haumarchaeota. *Environmental Microbiology*, 17(10), 3527–3539. <https://doi.org/10.1111/1462-2920.12508>
- Wei, Y., Wang, J., Liu, J., Dong, L., Li, L., Wang, H., et al. (2011). Spatial variations in archaeal lipids of surface water and core-top sediments in the South China Sea and their implications for paleoclimate studies. *Applied and Environmental Microbiology*, 77(21), 7479–7489. <https://doi.org/10.1128/AEM.00580-11>
- Weijers, J. W., Schouten, S., Spaargaren, O. C., & Damsté, J. S. S. (2006). Occurrence and distribution of tetraether membrane lipids in soils: Implications for the use of the TEX₈₆ proxy and the BIT index. *Organic Geochemistry*, 37(12), 1680–1693. <https://doi.org/10.1016/j.orggeochem.2006.07.018>
- Wuchter, C., Schouten, S., Wakeham, S. G., & Sinninghe Damsté, J. S. (2006). Archaeal tetraether membrane lipid fluxes in the north-eastern Pacific and the Arabian Sea: Implications for TEX86 paleothermometry. *Paleoceanography*, 21, PA4208. <https://doi.org/10.1029/2006PA001279>
- Xing, L., Zhang, R., Liu, Y., Zhao, X., Liu, S., Shi, X., & Zhao, M. (2011). Biomarker records of phytoplankton productivity and community structure changes in the Japan Sea over the last 166 kyr. *Quaternary Science Reviews*, 30(19–20), 2666–2675. <https://doi.org/10.1016/j.quascirev.2011.05.021>
- Yamamoto, M., Kishizaki, M., Oba, T., & Kawahata, H. (2013). Intense winter cooling of the surface water in the northern Okinawa Trough during the last glacial period. *Journal of Asian Earth Sciences*, 69, 86–92. <https://doi.org/10.1016/j.jseas.2012.06.011>
- Yokoyama, Y., Kido, Y., Tada, R., Minami, I., Finkel, R. C., & Matsuzaki, H. (2007). Japan Sea oxygen isotope stratigraphy and global sea-level changes for the last 50,000 years recorded in sediment cores from the Oki Ridge. *Palaeogeography, Palaeoclimatology, Palaeoecology*, 247(1–2), 5–17. <https://doi.org/10.1016/j.palaeo.2006.11.018>
- Zhang, Y. G., & Liu, X. (2018). Export depth of the TEX₈₆ signal. *Paleoceanography and Paleoclimatology*, 33(7), 666–671. <https://doi.org/10.1029/2018PA003337>
- Zhang, Y. G., Pagani, M., & Wang, Z. (2016). Ring Index: A new strategy to evaluate the integrity of TEX₈₆ paleothermometry. *Paleoceanography*, 31, 220–232. <https://doi.org/10.1002/2015PA002848>
- Zou, J., Shi, X., Liu, Y., Liu, J., Selvaraj, K., & Kao, S. J. (2012). Reconstruction of environmental changes using a multi-proxy approach in the Ulleung Basin (Sea of Japan) over the last 48 ka. *Journal of Quaternary Science*, 27(9), 891–900. <https://doi.org/10.1002/jqs.2578>

References From the Supporting Information

- Jo, C. O., Park, S., Kim, Y. H., Park, K.-A., Park, J. J., Park, M.-K., et al. (2014). Spatial distribution of seasonality of SeaWiFS chlorophyll-a concentrations in the East/Japan Sea. *Journal of Marine Systems*, 139, 288–298. <https://doi.org/10.1016/j.jmarsys.2014.07.004>
- Kim, H.-C., & Yoo, S. (2007). Relationship between phytoplankton bloom and wind stress in the sub-polar frontal area of the Japan/East Sea. *Journal of Marine Systems*, 67(3–4), 205–216. <https://doi.org/10.1016/j.jmarsys.2006.05.016>
- Nakanishi, T., Yamamoto, M., Tada, R., & Oda, H. (2012). Centennial-scale winter monsoon variability in the northern East China Sea during the Holocene. *Journal of Quaternary Science*, 27(9), 956–963. <https://doi.org/10.1002/jqs.2589>
- Prahl, F. G., & Wakeham, S. G. (1987). Calibration of unsaturation patterns in long-chain ketone compositions for palaeotemperature assessment. *Nature*, 330(6146), 367–369. <https://doi.org/10.1038/330367a0>
- Yamada, K., Ishizaka, J., Yoo, S., Kim, H.-C., & Chiba, S. (2004). Seasonal and interannual variability of sea surface chlorophyll a concentration in the Japan/East Sea (JES). *Progress in Oceanography*, 61(2–4), 193–211. <https://doi.org/10.1016/j.pocean.2004.06.001>